ACADEMIC PRESS

Available online at www.sciencedirect.com
SCIENCE DIRECT®

Journal of Catalysis 215 (2003) 57–65

JOURNAL OF CATALYSIS

www.elsevier.com/locate/jcat

Structure–reactivity correlations in sulphated-zirconia catalysts for the isomerisation of α-pinene

Muriel A. Ecormier,[a] Karen Wilson,[b] and Adam F. Lee [a,*]

[a] *Department of Chemistry, University of Hull, Hull HU6 7RX, UK*
[b] *Department of Chemistry, University of York, Heslington, York YO10 5DD, UK*

Received 5 August 2002; revised 7 October 2002; accepted 4 November 2002

Abstract

A range of mesoporous sulphated zirconias with tuneable structural and catalytic properties have been prepared by direct impregnation. The surface sulphate coverage can be readily varied, achieving a maximum value of ~ 0.2 monolayers. High-temperature calcination induces the crystallisation of tetragonal zirconia while suppressing the monoclinic phase and enhances surface acidity. Superacid sites only appear above a critical threshold SO_4 coverage of 0.08 mL (corresponding to 0.44 wt% total S). Sulphated zirconias show good activity towards α-pinene isomerisation of under mild conditions. Conversion correlates with the number Brønsted acid sites, while the selectivity towards mono- versus polycyclic products depends on the corresponding acid site strength; superacidity promotes limonene formation over camphene.

Keywords: Solid acid catalysts; Clean technology; Green chemistry; Zirconia; α-pinene

1. Introduction

The syntheses of many fine and speciality chemicals often rely on homogeneous mineral acids, bases, or metal salts, which are frequently used in stoichiometric amounts. Tightening legislation on the treatment and disposal of excessive toxic waste, produced during the separation and neutralisation of products from these reaction media, is driving industry to consider cleaner technologies, including the use of heterogeneous catalysis. Of particular concern are the wide range of liquid-phase industrial reactions which rely on the use of inorganic or mineral acids. While many of these processes are catalytic, some require stoichiometric amounts of acid (e.g., acylation using $AlCl_3$). While zeolites are widely employed as solid acid catalysts in gas-phase chemistry, their application in liquid-phase organic synthesis is limited by their small pore sizes (< 8 Å), which make them unsuitable for reactions involving bulky substrates. However, recent developments in materials chemistry have led to the discovery of the M41S family of mesoporous molecular sieves [1,2] offering pore sizes in the range 20–100 Å and thus new avenues for liquid-phase solid acid catalysis.

In contrast to liquid acids, which possess well-defined acid properties, solid acids may contain a variety of acid sites. Generally they are categorised by their Brønsted and/or Lewis acidity, the strength and number of these sites, and the textural properties of the support (surface area and porosity) [3]. The synthesis of pure Brønsted and pure Lewis acid catalysts has attracted great academic interest, although the latter has proven more difficult because Brønsted acidity often arises from Lewis acid–base complexation [4]. In order to achieve high selectivity towards the desired products in a synthesis all these properties must be considered and if possible controlled. For example, acetal formation and hydrolysis reactions generally require medium-acid-strength sites, while electrophilic additions of alcohols or water to olefins, skeletal rearrangements, and esterification and alkylation reactions require strong acid sites. The importance of the type of acid site has likewise been shown for Friedel Crafts alkylation reactions, where Lewis acid sites are required for toluene alkylation by benzyl chloride, while Brønsted sites are preferred for reactions using benzyl alcohol [5].

There has been much interest in the use of sulphated metal oxides as strong solid acids, in particular sulphated

* Corresponding author.
E-mail address: a.f.lee@chem.hull.ac.uk (A.F. Lee).

0021-9517/03/$ – see front matter
doi:10.1016/S0021-9517(02)00150-1

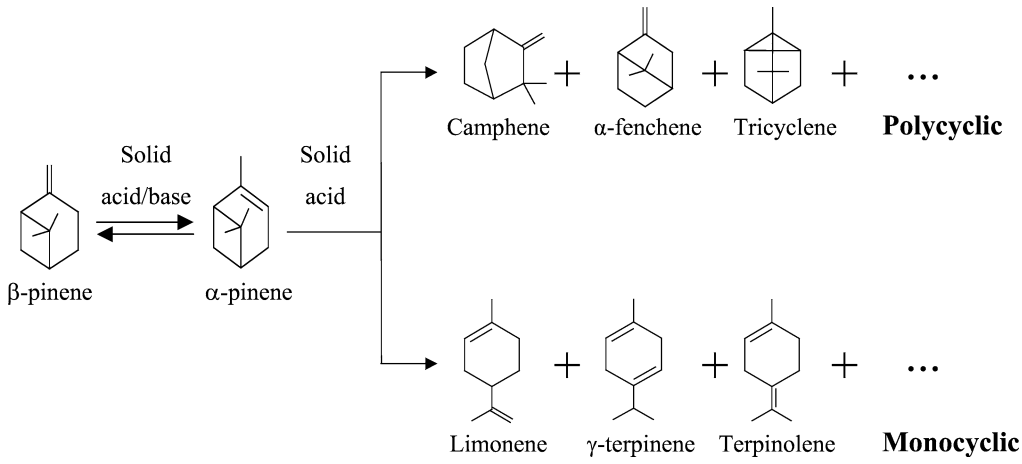

Scheme 1.

zirconias, which have been suggested to possess superacidic properties [6]. While most research has focused on gas-phase transformations [7,8] for applications in cracking and isomerisation reactions, their use has been recently extended to liquid phase processes [9,10]. However, the nature of the active site(s) remains contentious, with both sol–gel and impregnation methods reported as effective preparation routes [11,12]. Sulphated zirconias' superacid nature has also been questioned; Hino and Arata first reported their low-temperature activity towards *n*-butane isomerisation [13] and evaluated their acid strength using Hammett indicators [14], the application of which to solids has been latterly criticised. A wide range of alternative techniques including NMR [15], NH_3 microcalorimetry [16,17], and ESR analysis [18] have been employed to address this issue; however, there is still no consensus. The super/strong acid sites, which are the active sites of the catalyst, have also been attributed to either Lewis [19,20], Brønsted [21,22], or a combination of both acid sites [23,24]. Alternative local zirconia geometries have also been postulated [7]. To our knowledge no systematic study of structure–reactivity relationships within these materials has been performed wherein acid strength has been correlated with SO_4 content and concomitant selectivity in liquid-phase chemistry.

To address this issue, we report the effect of controlled sulphation of a mesoporous ZrO_2 support on the structural, acidic, and catalytic properties of the resulting material. The rearrangement of α-pinene was selected to probe the effect of acid strength on catalytic performance [25]. This is a particularly interesting reaction as the product selectivity is known to vary with catalyst acid strength, with weak acids favouring camphene formation, while stronger acids result in monocyclic products [26,27], as shown in Scheme 1. The only previous study of this system, by Ponzi et al. [28,29], demonstrated that sulphated zirconias were active above 100 °C, producing mainly camphene. However, their catalysts were ill-defined and neither textural properties, surface sulphate loading, or acid strength were reported. Here we find that direct wet impregnation permits the preparation of mesoporous sulphated zirconias exhibiting tuneable surface acidity and concomitant selectivity control in the isomerisation of α-pinene under mild conditions.

2. Experimental

A series of sulphated zirconias were prepared by wet impregnation of 5 g zirconia (99%+, Engelhard) with 50 cm^3 of sulphuric acid (0.01–2.5 M). The resulting slurry was filtered and dried at 80 °C overnight before calcination at 550 °C for 3 h. The calcination temperature was selected to maximise the degree of surface ordering while minimising sulphur loss, based on the thermal analysis results presented in this paper. Samples were subsequently stored in air prior to characterisation and reactor testing.

Porosity and surface area measurements were performed following the N_2 adsorption on a Micromeritics ASAP 2010 instrument. Surface areas were calculated using the BET equation over the pressure range $P/P_0 = 0.02$–0.2, where a linear relationship was maintained, while pore size distributions were calculated using the BJH model. Sulphur content was determined by elemental analysis using a Carlo Erba 1108 CHN/S instrument; quoted percentages refer to total S levels. XPS measurements were performed using a Kratos AXIS HSi instrument equipped with a charge neutraliser and an Mg-K_α X-ray source. Spectra were recorded at normal emission using an analyser pass energy of 20 eV and X-ray power of 225 W. Two-point energy referencing was employed using adventitous carbon at 285 eV and the valence band. Ex situ XRD spectra were acquired by the use of a Siemens D5000 diffractometer and Cu-K_α radiation. The scan range was from $2\theta = 10°$ to 100° in increments of 0.02°. Peak-fitting was performed using a pseudo-Voigt function to determine crystallite sizes with the error estimated as ±10% for spherical/octahedral particles. Temperature-programmed reduction was carried out in a quartz tube using 50 mg of sample under a 5% H_2/N_2 flow

(E&W 99%) with a linear ramp rate of 11 °C min^{-1}. DRIFTS spectra were obtained using a Bruker Equinox FTIR spectrometer. Samples were diluted with KBr powder (10 wt% in KBr), then loaded into an environmental cell and subjected to additional drying under vacuum at 110 °C for 10 min prior to measurements to remove moisture physisorbed during air exposure. Ex situ pyridine adsorption was performed by incipient wetness impregnation, with excess pyridine evaporated prior to sample loading and evacuation as described above. Acidity was determined by Hammett indicators; ∼ 25 mg of sample was shaken with 1 cm^3 of a solution of Hammett indicator diluted in 10 cm^3 cyclohexane and left to equilibrate for 2 h. The colour on the catalyst was then noted. The following Hammett indicators were used: dicinnamalacetone ($pK_a = -3.0$), benzylacetophenone on chalcone ($pK_a = -5.6$), anthraquinone ($pK_a = -8.3$), 4-nitrotoluene ($pK_a = -11.35$), 3-nitrotoluene ($pK_a = -11.99$) and 2,4-dinitrotoluene ($pK_a = -13.75$). The acid strength is quoted as being stronger than the weakest indicator which exhibits a colour change, but weaker than the strongest base that produces no change.

Reactions were performed in a stirred batch reactor under nitrogen with samples being taken periodically for analysis using a Varian CP-3800 gas chromatograph fitted with a DB1 capillary column (film thickness 0.25 μm, id 0.32 mm, length 30 m) and a CP-8400 autosampler. The isomerisation of α-pinene was conducted at 60 °C using 63 mmol of α-pinene (98%, Aldrich), 100 mg of air-exposed catalyst, and 0.2 cm^3 of tetradecane (99%, Lancaster) as an internal standard. Reactions were run for 9 h with initial rates determined from the linear portion of the conversion profile. Catalyst selectivity and overall mass balances (closure was > 98%) were determined using appropriate reactant and product response factors derived from multipoint calibration curves. The systematic errors in the conversions and selectivities are ±2% and ±3%, respectively.

3. Results and discussion

The catalytic performance of sulphated zirconia hinges upon the successful incorporation of sulphoxy functionalities into the zirconia framework. Fig. 1 shows the total and surface sulphur content as a function of molarity of impregnating solution. It is evident that the total sulphur loading shows a rapid increase for low sulphuric acid concentrations (in line with the theoretical loading), demonstrating efficient S inclusion during the impregnation process. The surface sulphur levels were determined from the S2p XP intensity and overall surface composition, incorporating appropriate elemental response factors (RF) according to the equation

$$\mathrm{S\ (wt\%)} = \mathrm{I^S} \times \mathrm{RF^S} \big/ \big((I^{\mathrm{S}} \times \mathrm{RF^S}) + (I^{\mathrm{O}} \times \mathrm{RF^O}) \times (I^{\mathrm{Zr}} \times \mathrm{RF^{Zr}}) + (I^{\mathrm{C}} \times \mathrm{RF^C}) \big).$$

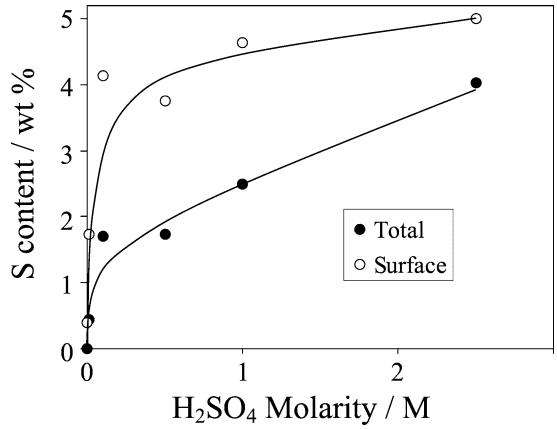

Fig. 1. Total and surface sulphur loading as a function of impregnating H_2SO_4 and molarity for calcined sulphated zirconias.

The surface loading mirrors the total sulphur content and exceeds it in all cases, as expected for an impregnation approach wherein only a small proportion should be incorporated within the bulk zirconia framework. Above > 1 M H_2SO_4 the surface loading begins to level off; however, the total loading continues to rise, approaching the final surface value of 5 wt% S for the 2.5 M treatment. Complete surface sulphation thus requires bulk sulphur loadings in excess of 1.7 wt%. These values represent the first quantitative determination of surface sulphur within sulphated zirconias.

Prior to calcination the impregnated samples possessed high surface areas, in excess of 250 m^2 g^{-1}, and showed a slight decrease with sulphur loading. Calcining at 550 °C reduced the surface areas of all samples (although they remain > 50 m^2 g^{-1} in all cases (Table 1). Pore size distribution measurements revealed that the resulting calcined materials were mesoporous (Fig. 2a), with well-defined pore sizes ranging between 33 and 46 Å reflecting the textural properties of the calcined ZrO_2 precursor (Fig. 2b). There was no systematic variation in pore diameter with sulphur content.

Fig. 3 shows the effect of calcination and sulphur loading on the thermal stability of impregnated zirconias as studied via temperature-programmed reduction (TPR). The zirconia precursor showed no reduction at temperatures below 700 °C, in accord with the literature [30,31]. Morterra et al. [32] reported that SO_2 is predominantly evolved during thermal reduction of sulphated zirconias; hence the peaks

Table 1
Influence of sulphur content and calcination on the surface area of sulphated zirconias

Total S content (wt%)	Uncalcined (m^{2}g^{-1})	550 °C Calcined (m^2 g^{-1})
0	453	56
0.44	435	97
1.71	376	141
1.74	393	147
2.49	349	128
4.03	246	125

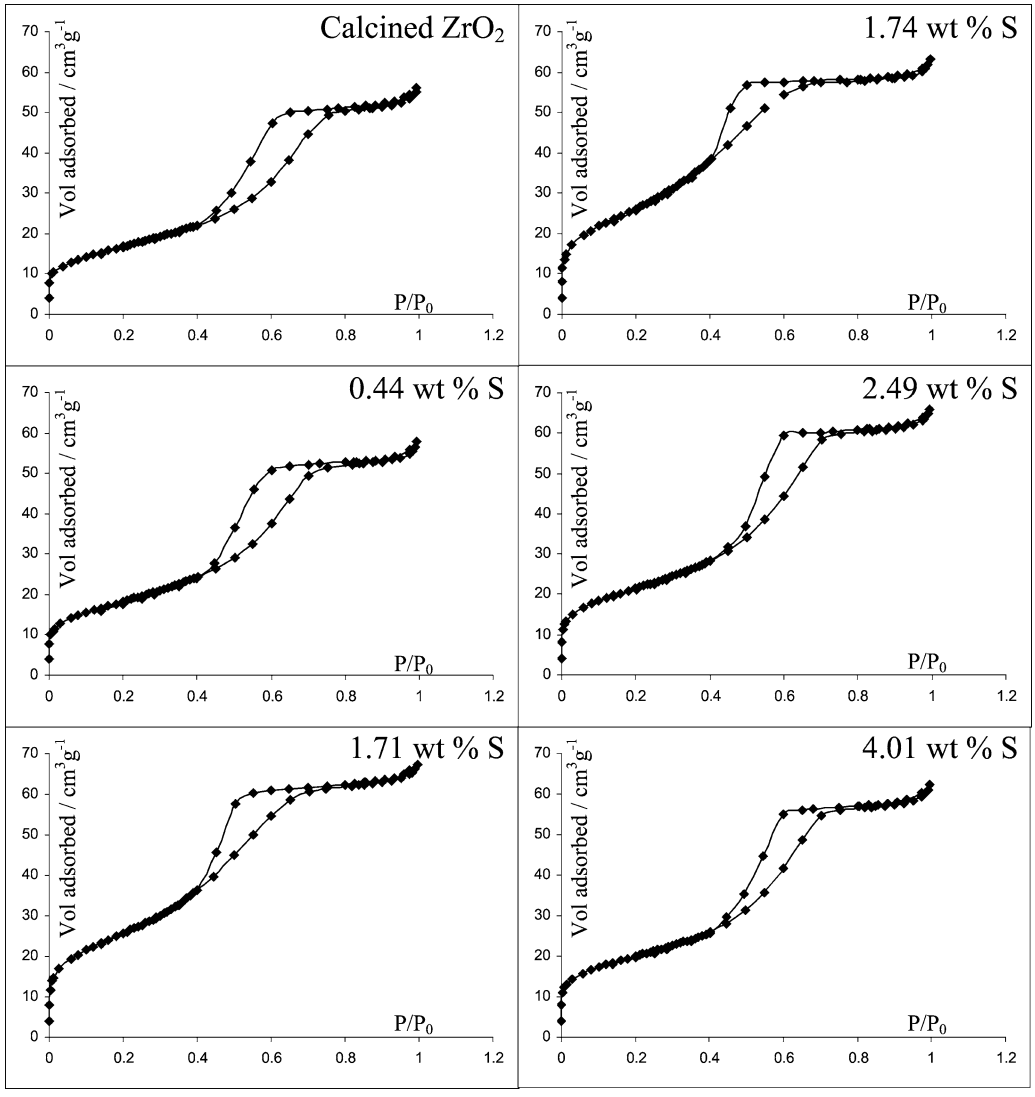

Fig. 2. (a) N_2 adsorption isotherms and (b) BJH pore-size distributions for calcined sulphated zirconias as a function of sulphur loading.

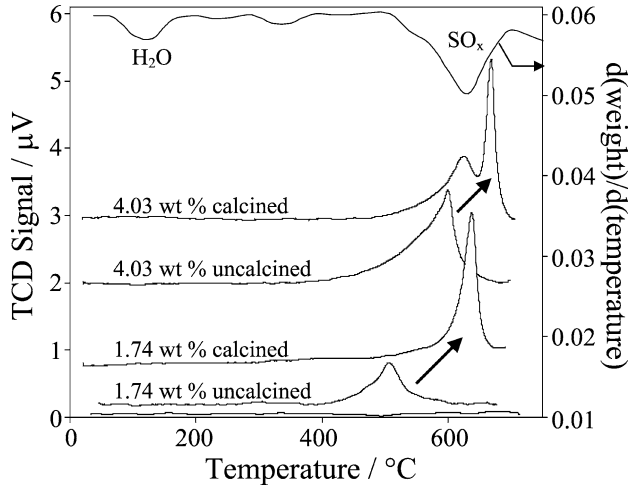

Fig. 3. Temperature-programmed reduction profiles for 1.74 and 4.03 wt% sulphated zirconias before and after 550 °C calcination. Corresponding differential thermogravimetric loss profile for the calcined 4.03 wt% sample is also shown.

observed between 400 and 700 °C for treated samples can be associated with the reduction of sulphoxy species. The calcination step increased the thermal stability of both low- and high-sulphur-loading materials. The TPR profile for the 1.74 wt% sample exhibits a single peak-indicating a relatively homogeneous sulphoxy environment. Although higher sulphur loadings led to increased thermal stability, they also reduced sample homogeneity, resulting in the emergence of a second, weaker reduction state ~ 50 °C the main peak. These observations suggest that a single SO_4 species predominates up to the saturation coverage determined by XPS, beyond which sulphur is incorporated within various subsurface environments. Corresponding thermogravimetric analysis confirmed the principal high temperature SO_x decomposition process and also identified a small mass loss at 100 °C associated with adsorbed water desorption.

The formation of crystalline sulphated zirconia via the impregnation process was explored using powder X-ray diffraction, Fig. 4. The uncalcined zirconia precursor contained only a single weak, broad reflection centred around $2\theta = 30°$, indicating essentially amorphous character and thus consistent with the porosimetry data. In contrast, the calcined zirconia support exhibited reflections arising from both monoclinic ($2\theta = 24.7°$, 28.4°, 31.6° [33]) and tetragonal ($2\theta = 30.3°$, 35.3°, 50.7°, 59.9°, 60.6° and 63.5° [34]) zirconia phases. All the sulphated materials were likewise highly ordered; however, increasing the sulphur loading above 0.44 wt% caused a sharp increase in the intensity of the tetragonal phase and concomitant loss of the monoclinic phase. Although sulphation was previously reported to induce a similar structural transformation in the support from amorphous to tetragonal zirconia [35], our results show that there is a threshold sulphur coverage for this evolution; loadings > 0.44 wt% are necessary to effect a complete monoclinic → tetragonal transition. Peak shape analysis showed that the tetragonal phase comprised small crystallites of ~ 145 Å independent of sulphur loading; high-temperature calcination (> 650 °C) has been shown to eliminate differences in sulphated-zirconia crystallite sizes [36]. The monoclinic phase present in the calcined and 0.44 wt% zirconia samples possessed a similar average crystallite size. It is interesting to note that sulphated zirconias prepared by sol–gel routes (with total loadings of 1.69 and 2.73 wt% S, respectively) gave diffractograms almost identical to those of the higher loading samples produced by direct impregnation and are similar to those previously observed [37,38]. Neither preparative route gave rise to crystalline, stoichiometric zirconium sulphate.

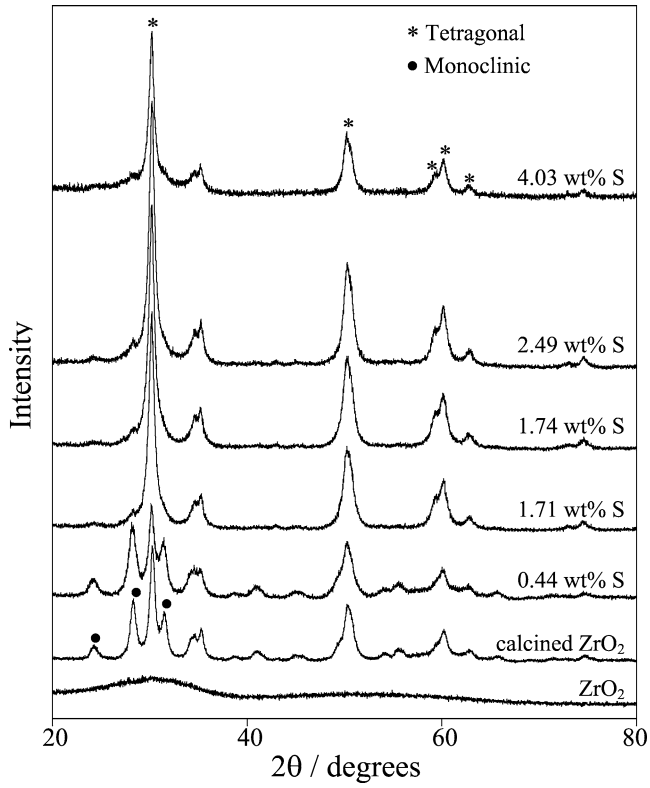

Fig. 4. X-ray diffractograms of calcined sulphated zirconias as a function of sulphur loading. The uncalcined zirconia support is shown for comparison.

The nature of the surface environment within both impregnated and sol–gel materials was explored by XPS. Zirconium 3*d* spectra (Fig. 5) of the calcined, unsulphated zirconia support showed a single poorly resolved doublet centred around 182.8 eV ($3d_{5/2}$) with a spin–orbit splitting of 2.4 eV. This binding energy is consistent with Zr^{IV} sites in ZrO_2 [39]. Sulphation resulted in a linear decrease in signal intensity (Fig. 5, inset) with the highest loading giving $\sim 30\%$ Zr attenuation, consistent with formation of a chemisorbed sulphoxy overlayer. This was accompanied by a slight Zr peak shift around 0.15 eV to higher binding energy, suggesting the direct coordination of zirconium atoms to strongly electron-withdrawing SO_x centres. Fig. 6 shows that the oxygen 1*s* spectrum for calcined, unsulphated zirconia comprises a single dominant peak at ~ 530.4 eV,

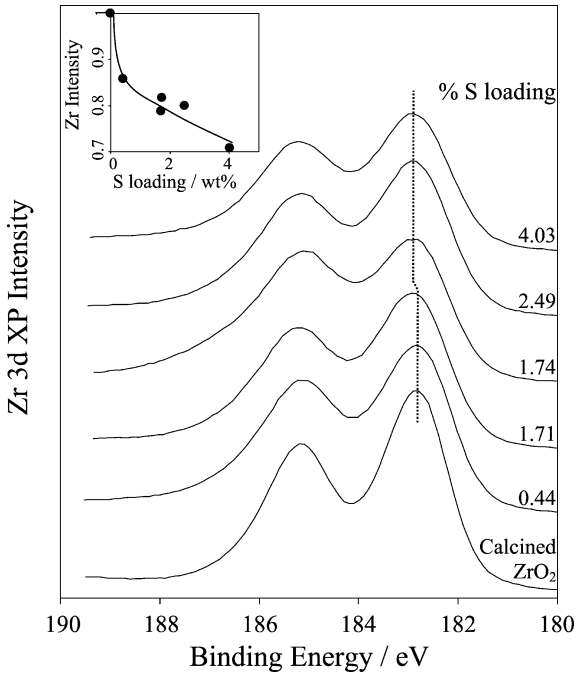

Fig. 5. Zr3*d* XP spectra of calcined sulphated zirconias as a function of sulphur loading. Inset shows normalised integrated Zr intensity versus loading.

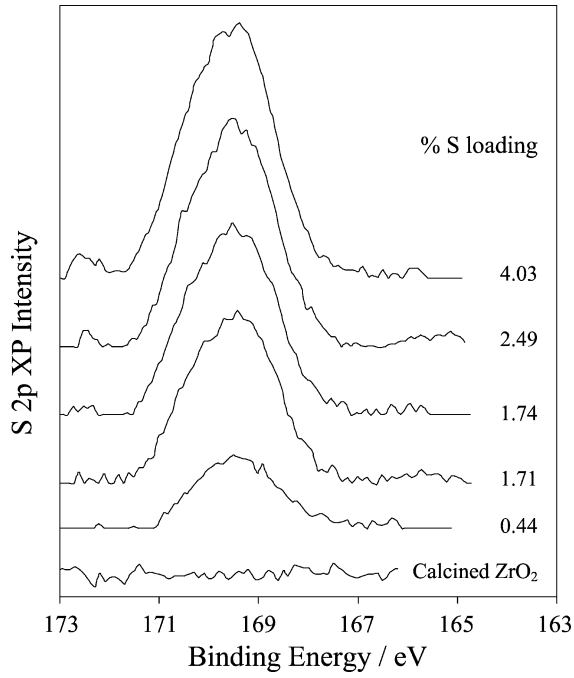

Fig. 7. S2*p* XP spectra of calcined sulphated zirconias as a function of sulphur loading.

consistent with literature values [40]. Sulphation resulted in the gradual attenuation of this principal zirconia state and concomitant growth of a new high-binding-energy feature at ∼ 532.3 eV. The separation of these oxygen states (∼ 1.9 eV) was independent of sulphur loading, indicating the formation of a common (higher sulphoxy [41]) surface species for all materials. These observations are supported by the sulphur 2*p* spectra (Fig. 7), which exhibit a single broad state at ∼ 169.4 eV, consistent with a unique SO_4 environment [41,42]. A full $Zr(SO_4)_2$ monolayer (ML) would contain ∼ 22.6 wt% S, much greater than the limiting value of 5 wt%, suggesting that a maximum of only one-fifth of the zirconia surface (corresponding to ∼ 0.2 mL) undergoes sulphation.

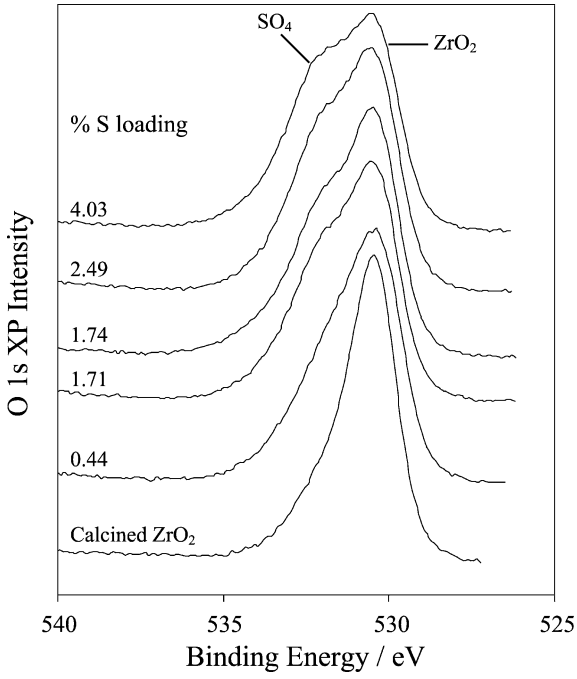

Fig. 6. O1*s* XP spectra of calcined sulphated zirconias as a function of sulphur loading.

Surface functionalisation of the calcined sulphated zirconias was further explored by DRIFTS. Sulphation resulted in the appearance of new features at ∼ 1625 cm^{-1} and in the region 1400–900 cm^{-1} (Fig. 8). The former peak arises from the δ_{HOH} bending mode of chemisorbed water coordinated to Lewis acid sites or hydrogen-bonded to polar sulphate/hydroxyl groups [43,44], while the latter region corresponds to the sulphoxy vibrations [45]. Higher sulphur loadings enhance the SO_x vibrational intensities but degrade their resolution, resulting in a broad spectral envelope for the 4.03 wt% sample. The principal SO_x components lie at 1240–1265 (S=O stretch), 1134–1152 (ν_s O=S=O), and 1045 cm^{-1} (S–O stretch). It is important to note the corresponding asymmetric O=S=O stretch, expected at ∼ 1300–1400 cm^{-1}, was of very low intensity, except for the lowest loading 0.44 wt% sample (indicative of bidentate sulphate [46,47]). The weakness of this band may reflect a reduced covalent character of the sulphoxy groups, as will be discussed later [46,48]. Pyridine adsorption was subsequently used to titrate Brønsted and Lewis acid sites. Fig. 9 shows the resulting DRIFTS spectra. As anticipated, the calcined zirconia precursor showed no detectable surface acidity, whereas all sulphated zirconias exhibited sharp peaks characteristic

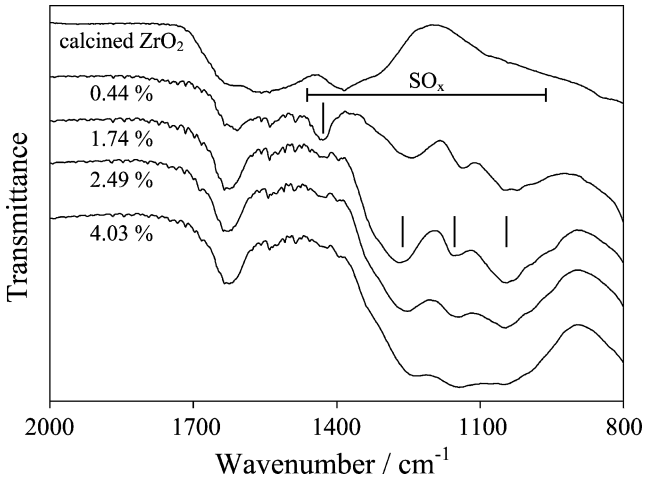

Fig. 8. DRIFTS spectra of calcined sulphated zirconias as a function of sulphur loading. The principal SO_x vibrations are indicated.

of predominantly Brønsted acid sites (1540 and 1633 cm^{-1}), although a small contribution from Lewis sites (1480 cm^{-1}) cannot be discounted [12,44,49]. A high concentration of Brønsted versus Lewis acid sites is to be expected as a result of moisture adsorption; Zhang et al. [50] have shown that $\sim 95\,\%$ of the total acid sites remain in Brønsted form after air-exposed sulphated zirconias are dried at 100 °C. The intensity of both acid features increases with sulphur loading, but rapidly plateaus, mirroring the surface sulphur content. Comparison with the uncalcined 4.03 wt% sample confirms that thermal processing improves the homogeneity of surface sulphate groups.

Fig. 10 presents the acid strength of the sulphated zirconias as estimated using Hammett indicators. Acid strength measurements using Hammett indicators rely on the use of a series of neutral basic indicators which change to the colour of their conjugate acid when interacting with acid sites of a critical pK_a. Quantitative acid site distributions can be determined by UV spectroscopy by titration of

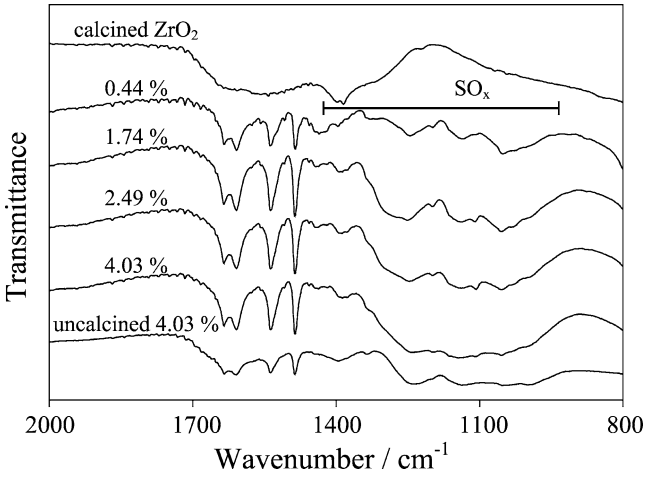

Fig. 9. DRIFTS spectra showing pyridine titration of calcined sulphated zirconias as a function of sulphur loading.

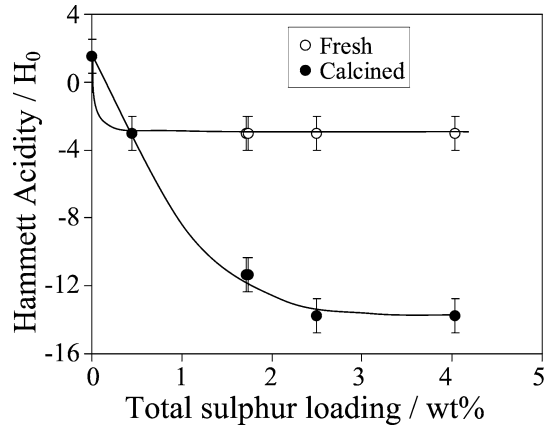

Fig. 10. Hammett acidity of fresh and calcined sulphated zirconias as a function of sulphur loading.

the suspended solid with *n*-butylamine, according to the Hammett–Bertolacini method [51]. However, determination of superacidity and acid site distributions of porous solid acid catalysts by such measurements remains controversial due to solvent–support interactions [52] and accessibility of the probe molecule within micropores [53]. Despite this, provided the polarity of the solvent used to suspend the solid and indicator is similar to that of the reaction media, semi-quantitative determination of the maximum solid acid strength can be obtained. From Fig. 10 uncalcined sulphated zirconias only displayed a marginal increase in the surface acidity of all samples, which remained weak solid acids. In contrast, subsequent calcination dramatically enhanced the resultant surface acidity, with superacidic properties emerging for bulk sulphur loadings > 1.71 wt%, which exhibited a limiting H_0 of between -12 and -13. It is interesting to note that the trend in H_0 exhibits a direct correspondence with the surface SO_4 coverage. The S XP spectra show no evidence for new chemically distinct SO_x species at high loadings; hence superacidity does not arise from a change in the S oxidation state or significant restructuring of the sulphate local environment.

The corresponding catalytic properties of the sulphated zirconias towards α-pinene isomerisation were subsequently explored. Fig. 11 shows that the calcined zirconia support possesses poor activity with a corresponding limiting conversion of only 5% after 9 h reaction. Sulphation enhances catalyst performance, with initial rates showing a direct correlation with measured surface sulphate coverage (ranging from ~ 0.08 to 0.2 ML SO_4) and thus acid site density. The intrinsic (area-normalised) catalyst activities are almost independent of sulphate loading and thus acid site strength at $\sim 0.35 \pm 0.05$ mmol h^{-1} $gcat^{-1}$ m^{-2}. Pinene conversion mirrored the activity trends with a maximum of 66% obtained for the 4.03 wt% catalyst. Sulphation also induces a significant switchover in selectivity from essentially pure polycyclic camphene over unsulphated zirconia towards the monocyclic limonene product, in striking agreement with the acid strength predictions from the Hammett indicators.

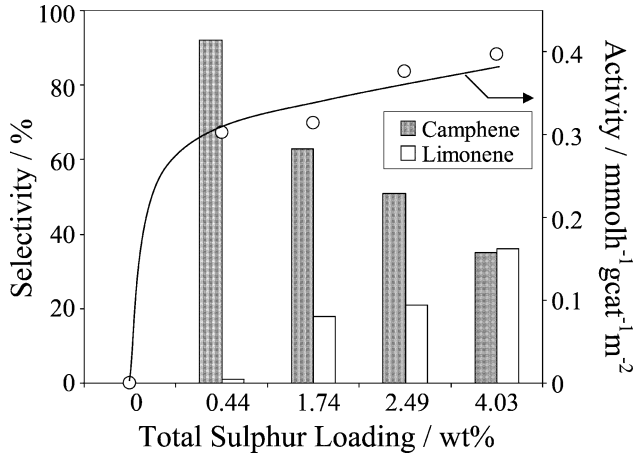

Fig. 11. Catalytic performance of calcined sulphated zirconias in α-pinene isomerisation after 9 h reaction as a function of sulphur loading. T_{reax} = 60 °C. Activities have been normalised to the BET surface areas.

Small amounts of α-terpinene, γ-terpinene, and p-cymene were also observed as residual secondary by-products, most notably for the superacidic catalysts.

The correlation between acidity and surface sulphate loading can be understood by considering the Clearfield model for acid site formation in sulphated zirconia. Exposure of ZrO_2 or $Zr(OH)_4$ surfaces to H_2SO_4 solutions is proposed to result in surface bisulphate groups (HSO_4^-) in a bidentate coordination. During subsequent calcination bisulphate can undergo condensation with adjacent hydroxyl groups to form a neutral bidentate sulphate species together with a Lewis acid centre located on the zirconia support (Scheme 2a). The latter can readily interconvert to yield weak Brønsted sites on coordination with water. Our structural measurements reveal that weak sulphuric acid solutions result in a low surface coverage of bidentate SO_4 groups exhibiting strong covalent character. The corresponding support shows incomplete crystallisation (Fig. 4, 0.44 wt% sample) and therefore partial hydration, consistent with a surface in which excess hydroxyl functionality was available for complete neutralisation of bisulphate.

As the H_2SO_4 concentration and thus initial bisulphate loading rise, the degree of reactive surface dehydroxylation is likewise expected to increase, as indeed evidenced by the appearance of the tetragonal phase of zirconia (usually formed via thermally dehydroxylation) for loadings $\geqslant$ 1.71 wt%. Above a critical bisulphate coverage there may be insufficient hydroxyl groups for the condensation reaction to proceed to completion during calcination. This would result in the stabilisation of permanently bound bisulphate Brønsted acid sites as postulated by Clearfield et al. [54] and Chen et al. [18] and the generation of new strong acid sites with an H_o value similar to that of sulphuric acid (Scheme 2b). Both our Hammett indicator measurements and the selectivity switchover from polycylic to monocylic products during α-pinene isomerisation support this model. The weaker covalent character of bisulphate versus sulphate would also account for loss of the asymmetric O=S=O stretch above 0.44 wt% S. Hence increasing the sulphate loading, and thus the surface bisulphate:hydroxyl ratio, seems to induce a transition from ZrO_2-derived weak Lewis/Brønsted acid sites to bisulphate-derived strong Brønsted acid sites.

4. Conclusions

Direct wet impregnation routes permit the synthesis of mesoporous sulphated zirconias with tuneable structural and catalytic properties. The molarity of H_2SO_4 impregnating solution controls the surface sulphate coverage, which attains a maximum of $\sim$ 0.2 ML SO_4 for acid concentrations $>$ 2.5 M. Sulphation induces a concomitant crystallisation of amorphous zirconia to the tetragonal phase, while suppressing the monoclinic phase, and the formation of superacidic sites. The emergence of these superacid sites above a critical threshold SO_4 coverage of 0.08 mL (0.44 wt% total S) appears associated with this bulk structural transformation and a corresponding change in the surface bisulphate concentration. Sulphated zirconias show good activity in the isomerisation of α-pinene, which has been successfully used to

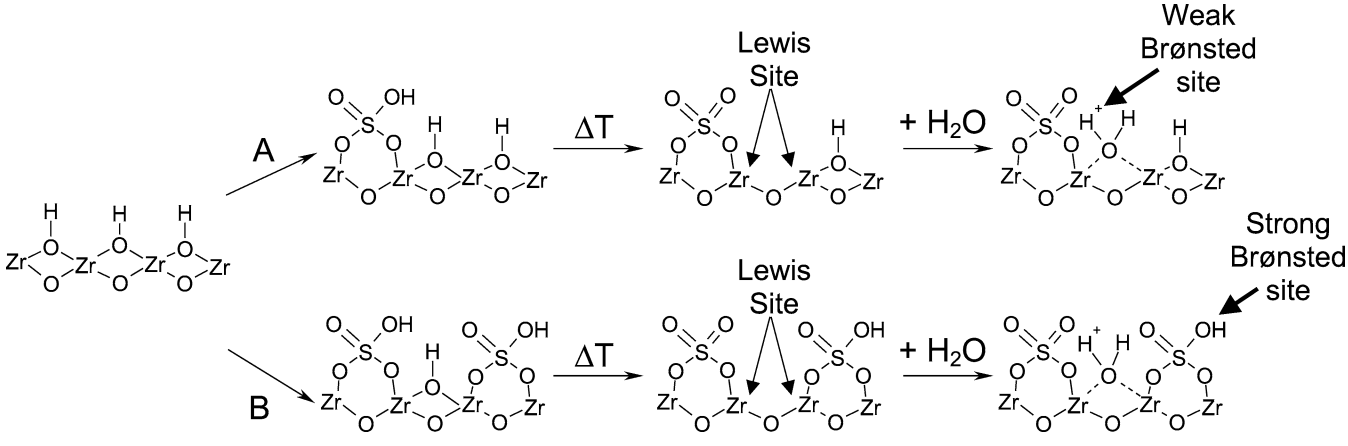

Scheme 2.

probe their surface acidity; low S loadings/weak acid sites favour camphene, while high S loadings/strong acid sites promote limonene production.

Acknowledgments

Financial support by the UK Engineering and Physical Sciences Research Council under Grant GR/M20877 and by BP-Amoco Chemicals is gratefully acknowledged. MAE thanks the University of Hull for financial assistance.

References

[1] J.S. Beck, J.C. Vartuli, W.J. Roth, M.E. Leonowicz, C.T. Kresge, K.D. Schmitt, C.T.-W. Chu, D.H. Olsen, E.W. Sheppard, S.B. McCullen, J.B. Higgins, J.L. Schlenker, J. Am. Chem. Soc. 114 (1992) 10834.
[2] U. Ciesla, M. Froba, G. Stucky, F. Schuth, Chem. Mater. 11 (1999) 227.
[3] K. Tanabe, M. Misono, Y. Ono, H. Hattori, New Solid Acids and Bases, in: Studies in Surface Science and Catalysis, Vol. 51, Elsevier, Amsterdam, 1998.
[4] K. Wilson, J.H. Clark, Pure Appl. Chem. 72 (2000) 1313.
[5] A. Corma, H. Garcia, Catal. Today 38 (1997) 257.
[6] K. Arata, Appl. Catal. A. 146 (1996) 3.
[7] X. Song, A. Sayari, Catal. Rev. 38 (1996) 329.
[8] Q.-H. Xia, H. Hidajat, S. Kawi, J. Catal. 205 (2002) 318.
[9] G.D. Yadav, J.J. Nair, Micropor. Mesopor. Mater. 33 (1999) 1.
[10] D.J. McIntosh, R.A. Kydd, Micropor. Mesopor. Mater. 37 (2000) 281.
[11] H. Armendariz, B. Coq, D. Tichit, R. Dutartre, F. Figueras, J. Catal. 173 (1998) 345.
[12] V. Parvulescu, S. Coman, P. Grange, V.I. Parvulescu, App. Catal. A Gen. 176 (1999) 27.
[13] M. Hino, K. Arata, J. Chem. Soc. Chem. Commun. (1980) 851.
[14] M. Hino, K. Arata, J. Am. Chem. Soc. 101 (1979) 6439.
[15] T. Riemer, D. Spielbauer, M. Hunger, G. Mekhemer, H. Knozinger, J. Chem. Soc. Chem. Commun. (1994) 1181.
[16] K.B. Fogash, G. Yaluris, M.R. Gonzalez, P. Ouraipryvan, D.A. Ward, E.I. Ko, J.A. Dumesic, Catal. Lett. 32 (1995) 241.
[17] G. Yaluris, R.B. Larson, J.M. Kobe, M.R. Gonzalez, K.B. Fogash, J.A. Dumesic, J. Catal. 158 (1996) 336.
[18] F.G. Chen, G. Coudurier, J.-F. Joly, J.C. Vedrine, J. Catal. 143 (1993) 616.
[19] M. Bensitel, O. Saur, J.-C. Lavalley, Mater. Chem. Phys. 17 (1987) 249.
[20] F. Pinna, M. Signoretto, G. Strukul, G. Cerrato, C. Morterra, Catal. Lett. 26 (1994) 339.
[21] R. Srinivasan, R.A. Keogh, B.H. Davis, Catal. Lett. 36 (1996) 51.
[22] F. Babou, B. Bigot, P. Sautet, J. Phys. Chem. 97 (1993) 11501.
[23] N. Katada, J. Endo, K. Notsu, N. Yasunobu, N. Naito, M. Niwa, J. Phys. Chem. B 104 (2000) 10321.
[24] B.H. David, R.A. Keogh, R. Srinivasan, Catal. Today 20 (1994) 219.
[25] J.C. van der Waal, H. van Bekkum, J.M. Vital, J. Mol. Catal. 105 (1996) 185.
[26] A. Stanislaus, L.M. Yeddanapalli, Canad. J. Chem. 50 (1972) 61.
[27] A. Severino, A. Esculcas, J. Roca, J. Vital, L.S. Lobo, Appl. Cat. A Gen. 142 (1996) 255.
[28] L. Grzona, N. Comelli, O. Masini, E. Ponzi, M. Ponzi, React. Kinet. Catal. Lett. 69 (2000) 271.
[29] N. Comelli, L. Grzona, O. Masini, E. Ponzi, M. Ponzi, React. Kinet. Catal. Lett. 71 (2000) 27.
[30] B.-Q. Xu, W.M.H. Sachtler, J. Catal. 167 (1997) 224.
[31] G. Delahay, E. Enusque, B. Coq, F. Figueras, J. Catal. 175 (1998) 7.
[32] C. Morterra, G. Cerrato, S. Di Ciero, M. Signoretto, F. Pinna, G. Strukul, J. Catal. 165 (1997) 172.
[33] E.A. Garcia, E.H. Rueda, A.J. Rouco, Appl. Catal. A Gen. 210 (2001) 363.
[34] T. Yamamoto, T. Tanaka, S. Takenaka, S. Yoshida, T. Onari, Y. Takahashi, T. Kosaka, S. Hasegawa, M. Kudo, J. Phys. Chem. B 103 (1999) 2385.
[35] C. Morterra, G. Cerrato, C. Emanuel, V. Bolis, J. Catal. 142 (1993) 349.
[36] M. Benaissa, J.G. Santiesteban, G. Diaz, C.D. Chang, M. Jose-Yacaman, J. Catal. 161 (1996) 694.
[37] A.F. Bedilo, K.J. Klabunde, J. Catal. 176 (1998) 448.
[38] A. Minesso, F. Genna, T. Finooto, A. Baldan, A. Benedetti, J. Sol Gel Sci. Technol. 24 (2002) 197.
[39] A.E. Hughes, B.A. Sexton, J. Electron. Spectrosc. Relat. Phenom. 50 (1990) c15.
[40] J.L. Colon, D.S. Thakur, C.-Y. Yang, A. Clearfield, C.R. Martin, J. Catal. 124 (1990) 148.
[41] C.D. Wagner, A.V. Naumkin, A. Kraut-Vass, J.W. Allison, C.J. Powell, J.R. Rumble Jr., NIST Standard Reference Database 20, Version 3.2, 2002.
[42] C.D. Wagner, in: D. Briggs, M.P. Seah (Eds.), Practical Surface Analysis, Vol. 1, Wiley, Chichester, 1990.
[43] B. Li, R.D. Gonzalez, Catal. Today 46 (1998) 55.
[44] C. Morterra, G. Cerrato, J. Phys. Chem. 98 (1994) 12373.
[45] T. Jin, T. Yamaguchi, K. Tanabe, J. Phys. Chem. 90 (1986) 4794.
[46] F. Babou, G. Coudurier, J.C. Vedrine, J. Catal. 152 (1995) 341.
[47] T. Yamaguchi, T. Jin, T. Ishiba, K. Tanabe, Mater. Chem. Phys. 17 (1987) 3.
[48] E. Escalona Platero, M. Penarroya Mentruit, Catal. Lett. 30 (1995) 31.
[49] K.T. Wan, C.B. Khouw, M.E. Davis, J. Catal. 158 (1996) 311.
[50] C. Zhang, R. Miranda, B.H. Davis, Catal. Lett. 29 (1994) 349.
[51] L. Forni, Catal. Rev. 8 (1974) 65.
[52] D. Farcasiu, A. Ghenciu, G. Marino, K.D. Rose, J. Am. Chem. Soc. 119 (1997) 11826.
[53] B.C. Gates, T.K. Cheung, Top. Catal. 6 (1998) 41.
[54] A. Clearfield, G.P.D. Serrette, A.H. Khazi-Syed, Catal. Today 20 (1994) 295.